Available online at www.sciencedirect.com

ScienceDirect

Ceramics International 40 (2014) 3399–3410

CERAMICS INTERNATIONAL

www.elsevier.com/locate/ceramint

Multi-color emission tunability and energy transfer studies of $YAl_3(BO_3)_4:Eu^{3+}/Tb^{3+}$ phosphors

G.V. Lokeswara Reddy[a], L. Rama Moorthy[a,b], T. Chengaiah[a], B.C. Jamalaiah[a,c,*]

[a]Department of Physics, Sri Venkateswara University, Tirupati 517502, India
[b]Department of Physics, Chadalawada Venkata Subbaiah Engineering College, Tirupati 517506, India
[c]Department of Materials Engineering and Ceramics, CICECO, University of Aveiro, Aveiro 3810-193, Portugal

Received 3 September 2013; accepted 20 September 2013
Available online 27 September 2013

Abstract

A series of YAB:Eu^{3+}/Tb^{3+} co-activated phosphors of composition $Y_{(1-x-y)}Al_3(BO_3)_4:xEu^{3+}/yTb^{3+}$ ($x=0$, 0.3, 0.5, 1, 2% and $y=0.5\%$) were prepared by solid-state reaction method and their photoluminescence properties were characterized. Eu^{3+}/Tb^{3+} co-doped phosphors have shown their excellent luminescent properties in their respective emission regions. The YAB:2%Eu^{3+} phosphor under 395 nm excitation exhibited red luminescence with Commission International de l'Eclairagein chromaticity coordinates ($x=0.627$, $y=0.334$) which are close to an ideal red and commercial $Y_2O_3:Eu^{3+}$ red phosphor chromaticity coordinates. The emission color of Eu^{3+}/Tb^{3+} co-doped phosphors has been tuned from pale-green to white as a function of Eu^{3+}/Tb^{3+} concentration. Moreover, the Tb^{3+} acts as an efficient sensitizer and enhances the luminescence of Eu^{3+} by transferring absorbed excitation energy. The overlapping $^7F_0\rightarrow{}^5D_{3,2,1,0}(Eu^{3+})$; $^7F_1\rightarrow{}^5D_{1,0}(Eu^{3+})$; $^7F_2\rightarrow{}^5D_1(Eu^{3+})$ excitation and $^5D_3\rightarrow{}^7F_{5,4,3}$ (Tb^{3+}); $^5D_4\rightarrow{}^7F_{5,4}(Tb^{3+})$ emission transitions revealed the transfer of energy from Tb^{3+} to Eu^{3+} through exchange interaction mechanism in Eu^{3+}–Tb^{3+} clusters instead of from these ions randomly distributed in YAB lattice. The YAB:Eu^{3+}/Tb^{3+} phosphors have potential in the field of display technology.

Keywords: A. Powders: solid state reaction; B. Spectroscopy; C. Optical Properties; E. Display devices

1. Introduction

In recent years, the search for high efficiency, reliable, low power consumption and environmental friendly materials for white light-emitting diodes (w-LEDs) has become a proficient field. Up to now there are two different approaches for white light generation, the first one is a blue-LED chip combined with yellow phosphor (YAG:Ce) [1,2] and the other is a near ultraviolet (nUV) LED chip combined with tricolor (red/green/blue) phosphors [3,4]. Normally, w-LEDs with blue-LED chip have a low color rendering index due to the mixing of two colors and nUV-LED chip combined with tricolor phosphors has low luminescence efficiency. Moreover, single matrix tricolor phosphors have potential for white light-emitting sources due to their high luminescence efficiency and low manufacturing cost compared to the systems which require multiple phosphors to achieve the same effect [5]. Consequently, a novel and high luminescence efficiency white light source would be designed using UV-LED chip combined with single matrix phosphor doped with tricolor activators.

Rare earths (RE) doped yttrium based phosphors has potential applications in cathode radiation tube, field emission display and thin film electroluminescence devices due to their excellent chemical stability, low volatility in vacuum and absence of corrosive gas emission under electron bombardment [6–9]. The borate based phosphors activated with RE ions have prospective applications in the field of display technology owing to their high thermal and chemical stability [10,11]. The noncentrosymmetric $YAl_3(BO_3)_4$ (YAB) phosphor is of special interest due to the possibility of its wide isomorphous substitutions, luminescence and non-linear optical properties as a promising host lattice for RE activators. The structural, thermal and Fourier transform infrared (FTIR) analysis of YAB phosphor has been described in our earlier work [12]. It is well known that the luminescence efficiency of a phosphor depends strongly on crystal matrix of the host materials and influenced by the energy transfer (ET) process from host to

*Corresponding author at: Department of Materials and Ceramics Engineering, CICECO, University of Aveiro, Aveiro 3810-193, Portugal. Tel.: +351 923135265.
E-mail address: bcjamal@hotmail.com (B.C. Jamalaiah).

0272-8842/$ - see front matter © 2013 Elsevier Ltd and Techna Group S.r.l. All rights reserved.
http://dx.doi.org/10.1016/j.ceramint.2013.09.092

activator and/or sensitizer to activator. The ET process could be affected by the presence of carrier traps and/or defects in the host lattice. Thus, the trace co-dopant with different affinity has potential to change the trap configuration and consequently to improve the efficiency significantly [13,14]. From the literature it is clear that the Tb^{3+} acts as a good sensitizer to enhance the luminescence efficiency of Eu^{3+} ions in SrY_2O_4 [15], Y_2O_3 [16–18], $Na_3Gd(PO_4)_2$ [19] and $(YGd)BO_3$ [20] phosphors. Thus, the Tb^{3+} and Eu^{3+} ions could be used as efficient luminescent canters in display devices [21]. Depending on the concentration, the Tb^{3+} emits blue emission ($^5D_3 \rightarrow {}^7F_{3,4}$) at lower concentrations ($<0.5\%$) and green emission ($^5D_4 \rightarrow {}^7F_5$) at higher concentrations ($\geq 0.5\%$), while the Eu^{3+} ions emit red luminescence through $^5D_0 \rightarrow {}^7F_{0-6}$ transitions. This work concerns the preparation, photoluminescence, color tunability and energy transfer studies of YAB:Eu^{3+}/Tb^{3+} phosphors. The effect of Tb^{3+} sensitization on the luminescence of Eu^{3+} and the possible ways of transfer of energy from Tb^{3+} to Eu^{3+} were discussed.

2. Experimental

2.1. Materials and method

High-purity Y_2O_3 (99.99%), Al_2O_3 (99.9%), H_3BO_3 (99.5%), Eu_2O_3 (99.99%) and Tb_4O_7 (99.99%) from Sigma-Aldrich, India were used as starting materials. The YAB:Eu^{3+}/Tb^{3+} phosphors of composition $Y_{(1-x-y)}Al_3(BO_3)_4$: $x$$Eu^{3+}$/$y$$Tb^{3+}$ (x=0, 0.3, 0.5, 1, 2% and y=0.5%) were prepared by solid-state reaction method. Stoichiometric amounts of the starting materials were mixed homogeneously in the presence of acetone using a pestle and an agate mortar. An excess of 3% of H_3BO_3 was added to compensate its evaporation while heating. The samples were fired at 200 and 600 °C for 3 h and then sintered at 1200 °C for 3 h in CO atmosphere using alumina crucible.

2.2. Characterization

The X-ray diffraction (XRD) measurements were carried out on X'Pert-Pro Materials Research Diffractometer using CuKα radiation (λ=1.5406 Å). The photoluminescence excitation, emission and luminescence decay studies were recorded on a Jobin YVON Fluorolog-3 spectrofluorimeter. All the measurements were carried out at room temperature only.

3. Results and discussion

3.1. XRD analysis

The XRD profiles of pure, Eu^{3+}-, Tb^{3+}- and Eu^{3+}/Tb^{3+} co-doped YAB phosphors shown in Fig. 1a are appropriately consistent with JCPDS Card No. 72-1978. The YAB phosphor has huntite $CaMg_3(CO_3)_4$ structure with space group R32 and cell parameters: $a=b$=9.295 Å, c=7.243 Å, V=541.94 Å^3 [22,23]. The XRD profiles reveal that the intensity of observed XRD peaks decreases with the increase of concentration of dopant ions with their position remains unchanged. Taking into account the chemical valences and ionic radii (Y^{3+}: 0.090 nm; Eu^{3+}: 0.095 nm; Tb^{3+}: 0.092 nm), we suggest that the Tb^{3+} and Eu^{3+} ions substitute the Y^{3+} sites without disturbing the YAB crystal lattice. Negligibly weak YBO_3 phase might be due to boron loss at higher temperatures or the slower reaction rate of Al_2O_3 with Y_2O_3 and B_2O_3 [23,24]. The weak YBO_3 impure phase does not affect the optical properties of RE dopant present in YAB lattice [12]. The average crystallite size (D_{hkl}) of YAB:Eu^{3+}/Tb^{3+} phosphors has been calculated using the powder XRD data following the Scherer's formula [25] and the Hall–Williamsons equation [26]

$$D_{hkl} = \frac{0.89\lambda}{\beta_{2\theta} Cos\theta} \quad (1)$$

$$\frac{\beta_{2\theta} Cos\theta}{\lambda} = \frac{1}{D_{hkl}} + \frac{\varepsilon Sin\theta}{\lambda} \quad (2)$$

where λ is the wavelength of X-rays (1.5406 Å), $\beta_{2\theta}$ is the full width at half maximum and θ is the angle of diffraction. The constant ε represent the micro-strain present in the given phosphor. The average crystallite size of YAB:Eu^{3+}/Tb^{3+} phosphors is estimated to be ~56 nm from the Scherrer's formula (Eq. (1)). According to Hall–Williamsons equation (Eq. (2)), the reciprocal

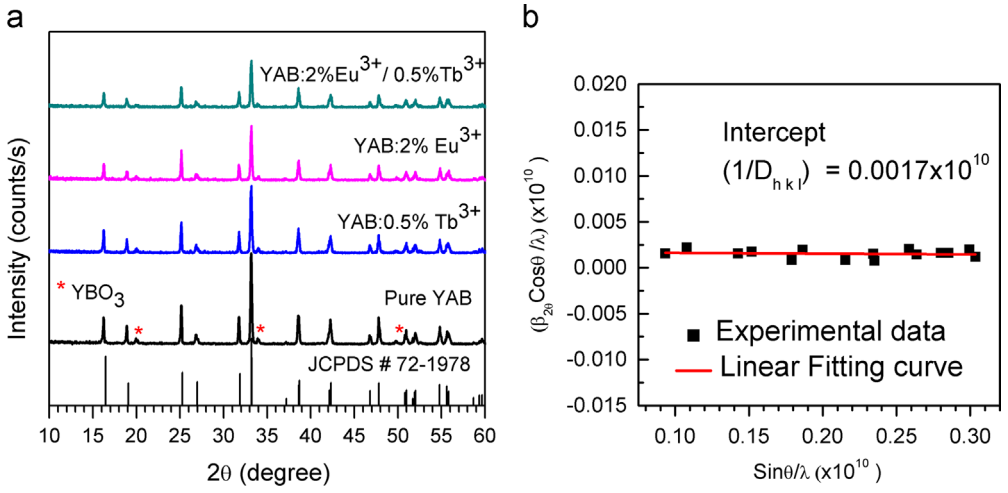

Fig. 1. XRD profiles for YAB:$x$$Eu^{3+}$/0.5%$Tb^{3+}$ phosphors (a) and Hall–Williamson plot for YAB:2%Eu^{3+}/0.5%Tb^{3+} phosphor (b).

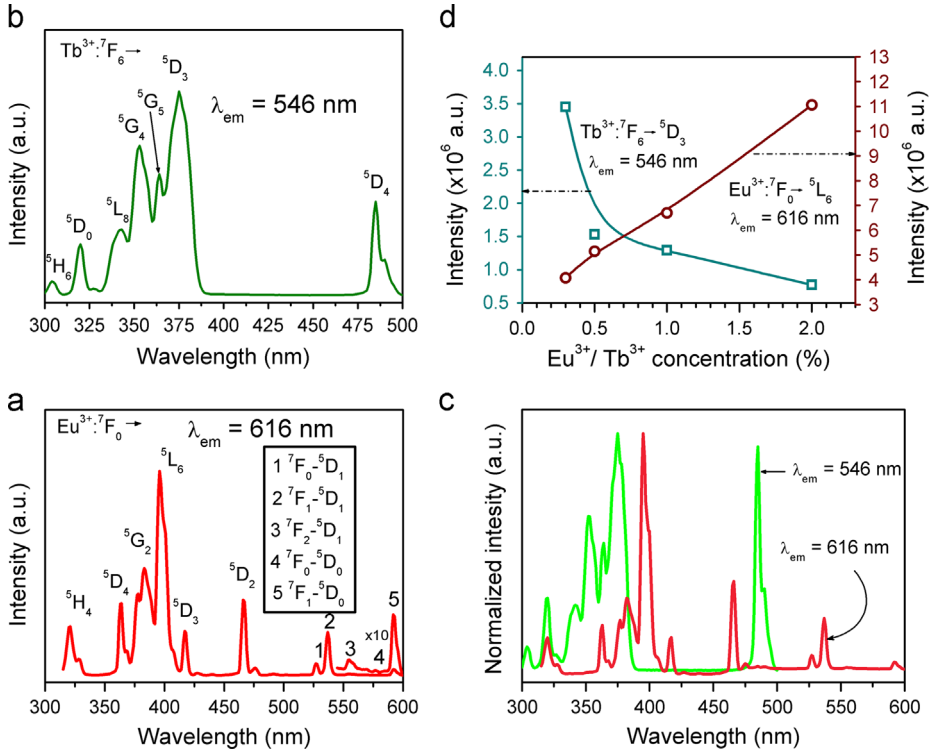

Fig. 2. PLE spectra of (a) 2%Eu^{3+}-, (b) 0.5%Tb^{3+}-, (c) 2%Eu^{3+}/0.5%Tb^{3+} co-doped YAB phosphors and (d) the variation of PLE intensity vs. Eu^{3+}/Tb^{3+} concentration.

of the intercept of $(\beta_{2\theta}\mathrm{Cos}\theta)/\lambda$ vs. $\mathrm{Sin}\theta/\lambda$ straight plot (Fig. 1b) gives the average crystallite size of ~58 nm which is very close to that calculated from the Scherrer's formula.

3.2. Photoluminescence excitation

The photoluminescence excitation (PLE) spectrum of YAB:2%Eu^{3+} phosphor monitoring the emission at 616 nm corresponding to the $^5D_0 \rightarrow {}^7F_2$ transition of Eu^{3+} shown in Fig. 2a exhibited eleven PLE bands due to the $^7F_0 \rightarrow {}^5H_4$ (320 nm), $^7F_0 \rightarrow {}^5D_4$ (363 nm), $^7F_0 \rightarrow {}^5G_2$ (382 nm), $^7F_0 \rightarrow {}^5L_6$ (395 nm), $^7F_0 \rightarrow {}^5D_3$ (417 nm), $^7F_0 \rightarrow {}^5D_2$ (466 nm), $^7F_0 \rightarrow {}^5D_1$ (527 nm), $^7F_1 \rightarrow {}^5D_1$ (537 nm), $^7F_2 \rightarrow {}^5D_1$ (554 nm), $^7F_0 \rightarrow {}^5D_0$ (576 nm) and $^7F_1 \rightarrow {}^5D_0$ (592 nm) transitions [27]. The PLE spectrum of YAB:0.5%Tb^{3+} phosphor with 546 nm emission due to the $^5D_4 \rightarrow {}^7F_6$ transition of Tb^{3+} (Fig. 2b) displayed a total of seven PLE bands corresponding to the $^7F_6 \rightarrow {}^5H_6$ (340 nm), $^7F_6 \rightarrow {}^5D_0$ (320 nm), $^7F_6 \rightarrow {}^5L_8$ (343 nm), $^7F_6 \rightarrow {}^5G_4$ (353 nm), $^7F_6 \rightarrow {}^5G_5$ (363 nm), $^7F_6 \rightarrow {}^5D_3$ (375 nm) and $^7F_6 \rightarrow {}^5D_4$ (485 nm) transitions [28]. Also, the PLE spectra of YAB:$x$$Eu^{3+}$/0.5%$Tb^{3+}$ phosphors were recorded by monitoring the emission of both Eu^{3+} ($^5D_0 \rightarrow {}^7F_2$; 616 nm) and Tb^{3+} ($^5D_4 \rightarrow {}^7F_6$; 546 nm) ions. These spectra are analogous to the corresponding Eu^{3+}- and Tb^{3+}- doped phosphors, respectively. For reference, the PLE spectra of YAB:2%Eu^{3+}/0.5% Tb^{3+} phosphor are described in Fig. 2c.

When the emission is monitored at main emission peak of Tb^{3+} ($^5D_4 \rightarrow {}^7F_6$; 546 nm) the intensity of PLE bands of Tb^{3+} decrease with the increase of Eu^{3+} concentration indicating the uniform distribution of Eu^{3+} and Tb^{3+} ions in YAB phosphors. Similarly, when the emission is monitored at prominent emission peak of Eu^{3+} ($^5D_0 \rightarrow {}^7F_2$; 616 nm) the intensity of PLE bands of Eu^{3+} increases monotonically with the increase of its concentration. The overlap of PLE bands (see Fig. 2c) of Eu^{3+} and Tb^{3+} in the spectral region 315–382 nm (~31,745–26180 cm^{-1}) suggest that the Tb^{3+} acts as a good sensitizer of luminescence for Eu^{3+} [29]. Further, the decrease in intensity of PLE transitions of Tb^{3+} with the increase of Eu^{3+} concentration is an indication of ET from Tb^{3+} to Eu^{3+}. The variation of intensity of Eu^{3+}:$^7F_0 \rightarrow {}^5L_6$ and Tb^{3+}:$^7F_6 \rightarrow {}^5D_3$ transitions as a function of Eu^{3+}/Tb^{3+} concentration is shown in Fig. 2d. As seen in Fig. 2a and b, the PLE bands with peak maximum at 395 nm (Eu^{3+}:$^7F_0 \rightarrow {}^5L_6$) and 375 nm ($Tb^{3+}$:$^7F_6 \rightarrow {}^5D_3$) are prominent when the main emission of Eu^{3+} ($^5D_0 \rightarrow {}^7F_2$; 616 nm) and Tb^{3+} ($^5D_4 \rightarrow {}^7F_6$; 546 nm) ions, respectively are monitored. Thus, the photoluminescence (PL) of YAB:Eu^{3+}/Tb^{3+} phosphors have been investigated under these two excitations only.

3.3. PL of Eu^{3+} and Eu^{3+}/Tb^{3+}

Fig. 3a presents the PL spectrum of YAB:2%Eu^{3+} phosphor excited under 395 nm. This figure displayed two groups of PL bands corresponding to the $^5D_1 \rightarrow {}^7F_{1,2}$ and $^5D_0 \rightarrow {}^7F_J$ (J=0,1,2,3,4) transitions. In case of Eu^{3+}, the $^5D_1 \rightarrow {}^7F_{1,2}$ emission transitions are insignificant and the $^5D_0 \rightarrow {}^7F_{0,1,2,3,4}$ transitions with peak maxima at 583, 596, 616, 656 and 701 nm, respectively are noteworthy. The PL spectra of YAB: $x$$Eu^{3+}$/0.5%$Tb^{3+}$ phosphors shown in Fig. 3b exhibited the similar emission transitions as that of YAB:2%Eu^{3+}. The emission mechanism of Eu^{3+} ion in YAB phosphors is

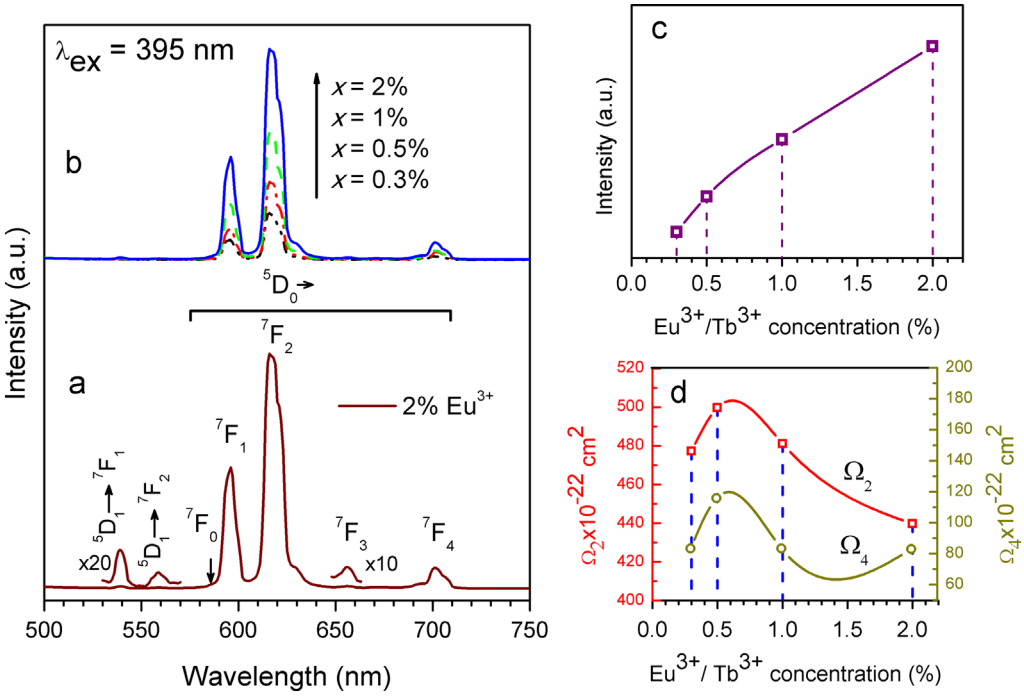

Fig. 3. PL spectra (λ_{ex}=395 nm) of (a) 2% Eu^{3+}-, (b) xEu^{3+}/0.5%Tb^{3+} co-doped YAB phosphors. The variation of intensity of Eu^{3+}:$^5D_0 \rightarrow {}^7F_2$ transition (c) and the *J–O* intensity parameters (d) as a function of Eu^{3+}/Tb^{3+} concentration.

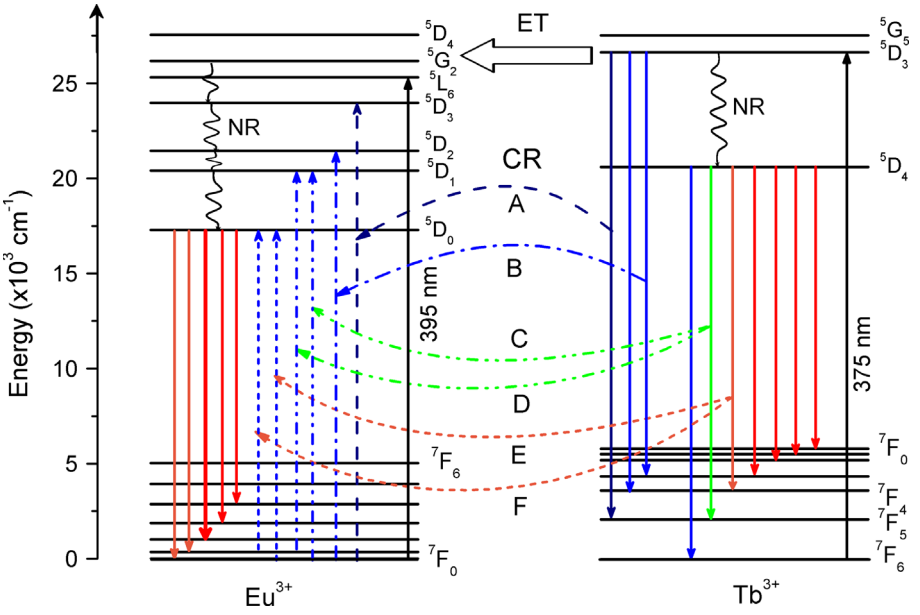

Fig. 4. Partial energy level diagram showing the emission mechanism, energy transfer and cross-relaxation channels in YA: xEu^{3+}/0.5%Tb^{3+} phosphors.

described in partial energy level diagram shown in Fig. 4. As seen in Fig. 3b, the intensity of Eu^{3+} emission transitions in Eu^{3+}/Tb^{3+} co-doped phosphors increases with the increase of Eu^{3+} ion concentration. The variation of intensity of Eu^{3+}:$^5D_0 \rightarrow {}^7F_2$ (616 nm) transition as a function of Eu^{3+}/Tb^{3+} concentration is shown in Fig. 3c. When the Eu^{3+} ions are pumped to any emission level above the $^5D_0$ state, a fast non-radiative (NR) multiphonon relaxation takes place to the $^5D_0$ level resulting $^5D_0 \rightarrow {}^7F_J$ radiative transitions by suppressing the other emissions related to the $^5D_{3,2,1} \rightarrow {}^7F_J$ transitions. Thus, the emission of Eu^{3+} ions has been considered as emission due to the $\Sigma^5D_0 \rightarrow {}^7F_J$. The multiphonon relaxation from $^5D_0$ level to its lower lying $^7F_6$ level is unlike due to the large energy gap of $\sim$12,260 cm^{-1}. Since, the maximum phonon energy of YAB lattice is $\sim$1354.72 cm^{-1} [12] nine phonons are required to bridge the energy gap between the $^5D_0$ and $^7F_6$ levels.

From the excitation (Fig. 3a) and emission (Fig. 4a) spectra of Eu^{3+} ion, the intensity of $^5D_0 \leftrightarrow {}^7F_0$ transition is found very weak showing the low symmetry local sites around the Eu^{3+} ion.

Table 1
The $\left(\frac{^5D_0 \rightarrow {}^7F_1}{^5D_0 \rightarrow {}^7F_2}\right)$ intensity ratios and the CIE chromaticity coordinates along with emission color for YAB:xEu^{3+}/0.5%Tb^{3+} phosphors under different excitation wavelengths.

Excitation wavelength	YAB doping	$\left(\frac{^5D_0 \rightarrow {}^7F_1}{^5D_0 \rightarrow {}^7F_2}\right)$	CIE coordinates		Emission color
			x-	y-	
395 nm	2% Eu^{3+}	0.36	0.627	0.334	Red
	x=0.3%	0.32	0.389	0.194	Purple
	x=0.5%	0.30	0.494	0.260	Pale-red
	x=1%	0.31	0.528	0.275	Pale-red
	x=2%	0.34	0.590	0.309	Red
375 nm	2% Eu^{3+}	0.32	0.577	0.301	Red
	x=0%	–	0.238	0.418	pale-green
	x=0.3%	0.56	0.236	0.293	Pale-blue
	x=0.5%	0.41	0.255	0.310	Pale-blue
	x=1%	0.36	0.314	0.323	Bluish-white
	x=2%	0.33	0.365	0.336	White

The intensity of $^5D_0 \rightarrow {}^7F_2$ electric dipole ($\Delta J=2$) transition is very sensitive and strongly influenced by the host environment while the intensity of $^5D_0 \rightarrow {}^7F_1$ magnetic dipole ($\Delta J=1$) transition is insensitive and hardly varies with the host environment. The $((^5D_0 \rightarrow {}^7F_1)/(^5D_0 \rightarrow {}^7F_2))$ intensity ratio gives the information regarding the site symmetry around the Eu^{3+} ion in which it is situated. Thus, the Eu^{3+} ion is therefore used often as the probe for local site symmetry [30]. When the Eu^{3+} ions occupy low symmetry sites, the intensity of $^5D_0 \rightarrow {}^7F_2$ electric dipole transition is often prominent than the $^5D_0 \rightarrow {}^7F_1$ magnetic dipole transition in its PL spectra and corresponding $((^5D_0 \rightarrow {}^7F_1)/(^5D_0 \rightarrow {}^7F_2))$ intensity ratio is less than unity. The $((^5D_0 \rightarrow {}^7F_1)/(^5D_0 \rightarrow {}^7F_2))$ intensity ratios determined from the PL spectra (λ_{em}=395 nm) are listed in Table 1. In the present investigation, the luminescence intensity of $^5D_0 \rightarrow {}^7F_2$ (616 nm) transition is found higher than that of $^5D_0 \rightarrow {}^7F_1$ (596 nm) transition and the relatively small $((^5D_0 \rightarrow {}^7F_1)/(^5D_0 \rightarrow {}^7F_2))$ intensity ratio (i.e., less than unity) indicates that the Eu^{3+} ions occupy low symmetry sites of YAB lattice.

The above discussion explore that the YAB:2%Eu^{3+} phosphor excited with 395 nm wavelength exhibit intense red luminescence with Commission International de l'Eclairagein (CIE) chromaticity coordinates (x=0.627, y=0.334), which are duly located in the red region of CIE chromaticity diagram shown in Fig. 5. The CIE chromaticity coordinates of YAB:Eu^{3+} phosphor are very close to an ideal red chromaticity coordinates (x=0.67, y=0.33) proposed by the National Television Standard Committee (NTSC), the commercial Y_2O_3:2%Eu^{3+} red phosphor (x=0.64, y=0.34) [KX-YOX, Kasei Optonix Ltd., Japan] and the most popularly used (Y,Gd)BO_3:Eu^{3+} red phosphor (x=0.65, y=0.35) [KX-504, Kasei Optonix Ltd., Japan]. The emission color of xEu^{3+}/0.5% Tb^{3+} co-doped phosphors varies from purple to red when the concentration of Eu^{3+} is raised from 0.3% to 2%. The CIE chromaticity coordinates and corresponding emission colors are also documented in Table 1. Upon 395 nm excitation, the tunable emission as a function of Eu^{3+}/Tb^{3+} concentration might be due to the defects and/or traps present in the YAB host lattice.

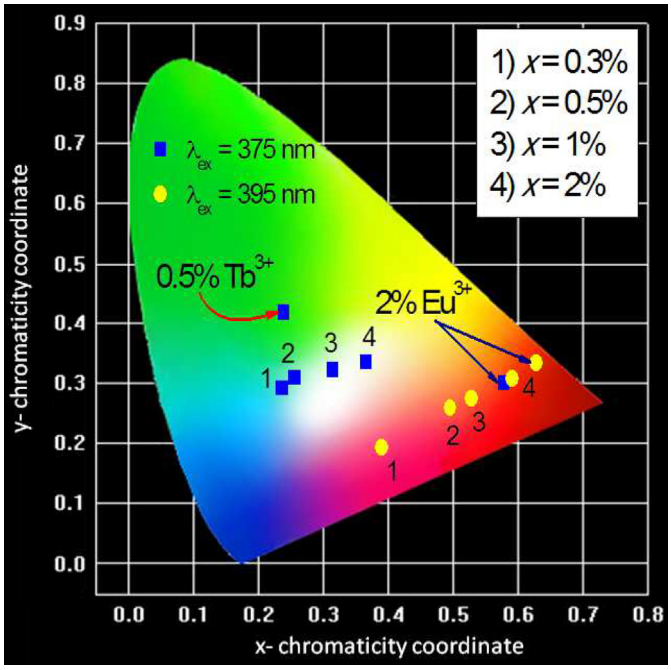

Fig. 5. CIE chromaticity diagram for 2% Eu^{3+}-, 0.5%Tb^{3+}- and xEu^{3+}/0.5% Tb^{3+} co-doped YAB phosphors under different excitation wavelengths.

3.4. Intensity parameters and radiative properties

The Judd-Ofelt (J-O) intensity parameters ($\Omega_{\lambda=2,4,6}$) has been calculated using the relation between $^5D_0 \rightarrow {}^7F_J$ (Eu^{3+}) emission transitions. These intensity parameters are then used

to evaluate the radiative transition rate, luminescence branching ratio and radiative lifetime. It is renowned that the intensity (I) of an emission transition is proportional to the radiative rate (A_{Rad}) of that transition. Also, it is proportional to the area (S) under that emission curve. Thus, the intensity of an emission transition can be written as follows:

$$I = (h\nu A_{Rad} N) \propto S \tag{3}$$

where h is the Planck's constant, ν is the energy separation between the initial and final levels and N is the population of the $^5D_0$ emitting level (in case of Eu^{3+}). The radiative transition rate is given by [31,32]

$$A_{Rad} = \frac{64\pi^4\nu^3}{3h(2J+1)}\left[\frac{n(n^2+2)^2}{9}\right]\sum_{\lambda}|\langle^5D_0||U^{(\lambda)}||^7F_\lambda\rangle|^2 \tag{4}$$

where $n(n^2+2)^2/9$ is the Lorentz local field correction factor which converts the external electromagnetic field into an effective field at the location of active center in the dielectric medium of refractive index 'n', $||U^{(\lambda)}||^2$ are the doubly reduced matrix elements and J is the total angular momentum of the initial state (emitting state). As the refractive index is wavelength dependent, taking the constant value into calculations result considerably small error in the evaluated Ω_λ intensity parameters in view of the fact that the refractive index changes are small over the wavelength region of interest (580–720 nm). For YAB lattice, the refractive index is ~1.70 [33]. The Ω_λ intensity parameters can be calculated using the following relation [34]:

$$\frac{\int I_\lambda d\nu}{\int I_1 d\nu} = \frac{e^2}{S_{md}}\left(\frac{\nu_\lambda}{\nu_1}\right)^3\frac{n(n^2+2)^2}{9n^3}\Omega_\lambda|\langle^5D_0||U^{(\lambda)}{}^7F_\lambda||\rangle|^2 \tag{5}$$

where $\int I_\lambda d\nu$ and $\int I_1 d\nu$ are the intensities of $^5D_0 \rightarrow {}^7F_\lambda$ (λ=2,4,6) and $^5D_0 \rightarrow {}^7F_1$ transitions, respectively. S_{md} is the magnetic dipole line strength for $^5D_0 \rightarrow {}^7F_1$ transition. ν_1 and ν_λ are the energies related to the $^5D_0 \rightarrow {}^7F_1$ and $^5D_0 \rightarrow {}^7F_\lambda$ transitions, respectively. In the present study, the value of (e^2/S_{md}) is taken as 2.47×10^{22}. Further, the Ω_λ intensity parameters have been computed by assuming the $||U^{(6)}||^2$ matrix element close to zero for $^5D_0 \rightarrow {}^7F_6$ transition ($|\langle^5D_0||U^{(6)}||^7F_6|\rangle|^2 = 0.0003$) and is equal to zero for other transitions. Also, the $^5D_0 \rightarrow {}^7F_6$ emission band has peak maximum at around 810–815 nm and in many cases it could not be observed due to the limitations of spectrofluorimeter. Thus, the Ω_2 and Ω_4 intensity parameters corresponding to the $^5D_0 \rightarrow {}^7F_2$ and $^5D_0 \rightarrow {}^7F_4$ transition has been determined by clearing the $||U^{(4)}||^2$, $||U^{(6)}||^2$ matrix elements for $^5D_0 \rightarrow {}^7F_2$ transition and $||U^{(2)}||^2$, $||U^{(6)}||^2$ matrix elements for $^5D_0 \rightarrow {}^7F_4$ transition taking $|\langle^5D_0||U^{(2)}||^7F_2\rangle|^2 = 0.0032$and $|\langle^5D_0||U^{(4)}||^7F_4\rangle|^2 = 0.0023$. For YAB:2%$Eu^{3+}$ phosphor, the J–O intensity parameters are $\Omega_2 = (4.16 \pm 0.20) \times 10^{-20}$ cm^2 and $\Omega_4 = (0.84 \pm 0.04) \times 10^{-20}$ cm^2 which are comparable to those reported for $ZnAl_2O_4$:Eu^{3+} [35] and $CaMoO_4$:Eu^{3+} [36] phosphors. The J–O intensity parameters of YAB:$x$$Eu^{3+}$/0.5%$Tb^{3+}$ phosphors are summarized in Table 2. As seen the Ω_λ intensity parameters one can notice that in case of YAB:Eu^{3+}/Tb^{3+} phosphors the magnitude of Ω_λ parameters increases with the increase of Eu^{3+} concentration up to 0.5% and then decrease for further increase of its concentration as described in Fig. 3d. The Ω_2 and Ω_4 intensity parameters are then used to evaluate the radiative transition rates (A_{Rad}) for the $^5D_0 \rightarrow {}^7F_J$ transitions using Eq. (4). In addition, the luminescence branching ratio (β_{Rad}) and the radiative lifetime (τ_{Rad}) have been calculated following the J–O theory [37,38]:

$$\beta_{Rad}(^5D_0 \rightarrow {}^7F_J) = \frac{A_{Rad}(^5D_0 \rightarrow {}^7F_J)}{\sum_J A_{Rad}(^5D_0 \rightarrow {}^7F_J)} \tag{6}$$

$$\tau_{Rad}(^5D_0) = \frac{1}{\sum_J A_{Rad}(^5D_0 \rightarrow {}^7F_J)} \tag{7}$$

The values of A_{Rad}, β_{Rad} and τ_{Rad} for $^5D_0 \rightarrow {}^7F_2$ (616 nm) transition of Eu^{3+} ion in YAB:$x$$Eu^{3+}$/0.5%$Tb^{3+}$ phosphors under 395 nm excitation are summarized in Table 2. The experimentally measured branching ratios (β_{meas}) determined from the relative areas under the emission bands are found to be in good agreement with the β_{Rad} (see Table 2). The magnitude of branching ratio is used to characterize the power of a stimulated emission transition and it is well established that an emission transition with branching ratio higher than 0.50 is more potential for stimulated emission. Theoretically predicted and experimentally measured branching ratio (~0.70) suggest that the YAB:$x$$Eu^{3+}$/0.5%

Table 2
J-O intensity parameters ($\Omega_{2,4}$), radiative properties and luminescence quantum efficiency (η_{QE}) for $^5D_0 \rightarrow {}^7F_2$ (616 nm) transition of Eu^{3+} ion in YAB:$x$$Eu^{3+}$/0.5% Tb^{3+} phosphors under 395 nm excitation.

Parameter	YAB:2% Eu^{3+}	YAB:$x$$Eu^{3+}$/0.5%$Tb^{3+}$ (λ_{ex}=395 nm)			
		x=0.3%	x=0.5%	x=1%	x=2%
Ω_2 ($\pm 0.20 \times 10^{-20}$ cm^2)	4.16	4.77	5.00	4.81	4.40
Ω_4 ($\pm 0.04 \times 10^{-20}$ cm^2)	0.84	0.83	1.16	0.83	0.83
$\Delta\lambda_{eff}$ (nm)	7.69	7.19	6.99	7.12	7.47
A_{Rad}(s^{-1})	190.53	218.58	228.91	220.39	201.42
β_{Rad}	0.69	0.72	0.71	0.72	0.70
β_{meas}	0.68	0.71	0.70	0.71	0.69
τ_{Rad}(ms)	3.61	3.28	3.10	3.26	3.48
σ_{emis}($\times 10^{-21}$ cm^2)	1.64	2.01	2.17	2.05	1.78
τ_{meas}(ms)	1.40	2.02	1.99	1.80	1.40
η_{QE}(%)	39	61	64	55	40

Tb^{3+} phosphors are appropriate for display devices. The emission cross-section (σ_{emis}) is one of the important optical parameter used to predict an active medium for stimulated emission.

$$\sigma_{emis}({}^5D_0 \rightarrow {}^7F_J) = \frac{\lambda_P^4}{8\pi c n^2 \Delta\lambda_{eff}} A_{Rad}({}^5D_0 \rightarrow {}^7F_J) \quad (8)$$

where λ_P is the peak emission wavelength, c is the speed of light and $\Delta\lambda_{eff}$ is the effective linewidth of the transition which can be determined using the equation: $\Delta\lambda_{eff} = \int I d\lambda / I_P$, here I_P is the intensity of corresponding transition. The evaluated values of $\Delta\lambda_{eff}$ and σ_{emis} are also listed in Table 2. As seen the emission cross-sections, the studied phosphors show emission with $\sigma_{emis} \approx 2.00 \times 10^{-21}$ cm^2.

3.5. Luminescence decay and quantum efficiency

The luminescence decay profiles of Eu^{3+}:$^5D_0$ emission state in YAB:2%Eu^{3+} and YAB:xEu^{3+}/0.5%Tb^{3+} phosphors with 616 nm emission and 395 nm excitation are shown in Fig. 6a and b, respectively. All the decay curves are well fitted to a single exponential equation, $I = I_0 e^{-t/\tau}$, where I is the intensity at time t, I_0 is the initial intensity when $t=0$ and τ is the lifetime. The experimentally measured (τ_{meas}) lifetime values have been obtained by taking the first e-folding times of the intensity of decay curves. The gradual decrease in lifetime with the increase of Eu^{3+} concentration (see Fig. 6c) is mainly due to the self quenching of Eu^{3+} ions at higher concentration [39]. The luminescence quantum efficiency (η_{QE}) is the most significant parameter used to predict stimulated emission transition is given as

$$\eta_{QE} = \frac{\tau_{meas}}{\tau_{Rad}} \quad (9)$$

The values of τ_{meas} and η_{QE} are given in Table 2. Based on the evaluated values of branching rations, stimulated emission cross-sections and the intrinsic quantum efficiencies we suggest that the YAB:xEu^{3+}/0.5%Tb^{3+} phosphors exhibit intense emission with luminescence efficiency higher than that of $CaMoO_4$:Eu^{3+} (12.78%) [36] and $Y_2(MoO_4)$:Eu^{3+} (22.38%) [39] phosphors.

3.6. PL of Tb^{3+} and Eu^{3+}/Tb^{3+}

The PL spectrum of YAB:0.5%Tb^{3+} phosphor under 375 nm excitation shown in Fig. 7a reveals two groups of PL bands originating from $^5D_3$ and $^5D_4$ emission levels to their ^7F_J lower lying levels. The emission bands corresponding to the $^5D_3 \rightarrow {}^7F_{5,4,3}$ transitions are centered at 417, 440 and 458 nm, respectively are insignificant in the present study due to their weak intensity, whereas the $^5D_4 \rightarrow {}^7F_{6,5,4,3}$ transitions with peak maxima at 490, 546, 595 and 623 nm, respectively are significant. This could be due to the higher concentration (0.5%) effect of Tb^{3+} only. When the samples are excited within Tb^{3+} ion ($^7F_6 \rightarrow {}^5D_3$; λ_{ex}=375 nm), the PL spectrum of YAB:2%Eu^{3+} phosphor shown in Fig. 7b is similar to that excited within Eu^{3+} ion ($^7F_0 \rightarrow {}^5L_6$; λ_{ex}=395 nm) (see Fig. 3a). Conversely, the YAB:xEu^{3+}/0.5% Tb^{3+} phosphors exhibit $^5D_3 \rightarrow {}^7F_{5,4,3}$ (Tb^{3+}); $^5D_4 \rightarrow {}^7F_{6,5}$ (Tb^{3+}) and $^5D_0 \rightarrow {}^7F_{1,2,4}$ (Eu^{3+}) transitions in blue, green and red emission regions, respectively as illustrated in Fig. 7c. Among these, the Tb^{3+}:$^5D_4 \rightarrow {}^7F_6$ (490 nm), Tb^{3+}:$^5D_4 \rightarrow {}^7F_5$ (546 nm) and Eu^{3+}:$^5D_0 \rightarrow {}^7F_2$ (616 nm) transitions are more prominent in YAB phosphors. As seen in Fig. 7c, the PL bands due to Tb^{3+}:$^5D_4 \rightarrow {}^7F_{4,3}$ and Eu^{3+}:$^5D_0 \rightarrow {}^7F_{1,2}$ transitions are overlapped. Further, with the increase of Eu^{3+} concentration the intensity of

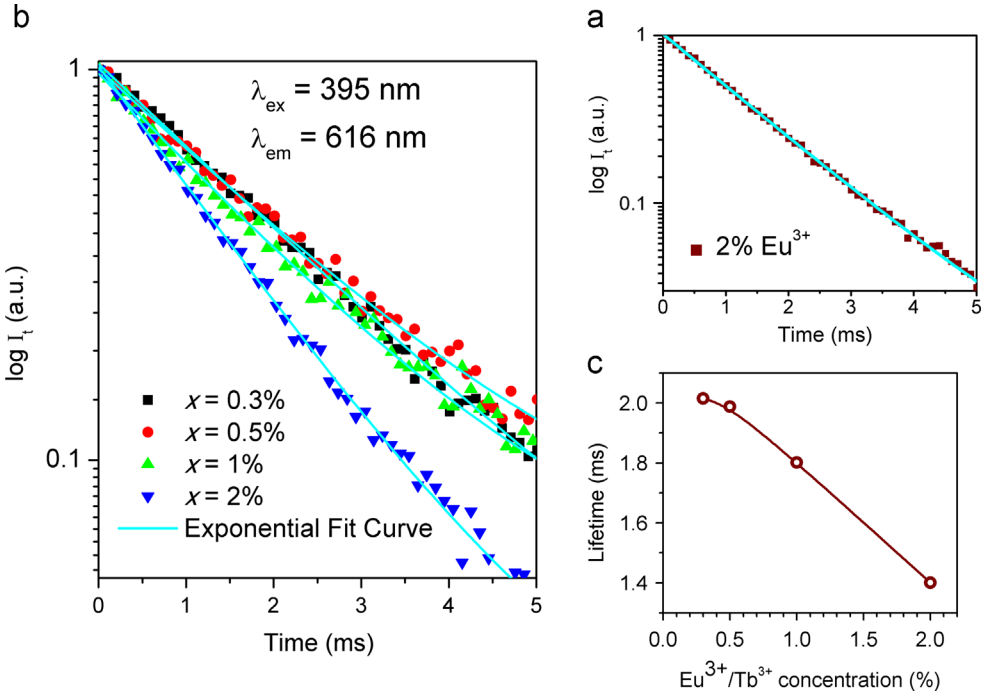

Fig. 6. Luminescence decay profiles of (a) 2%Eu^{3+}-, and (b) xEu^{3+}/0.5%Tb^{3+} co-doped phosphors. Figure (c) is the lifetime of $^5D_0$ (Eu^{3+}) state vs. Eu^{3+}/Tb^{3+} concentration.

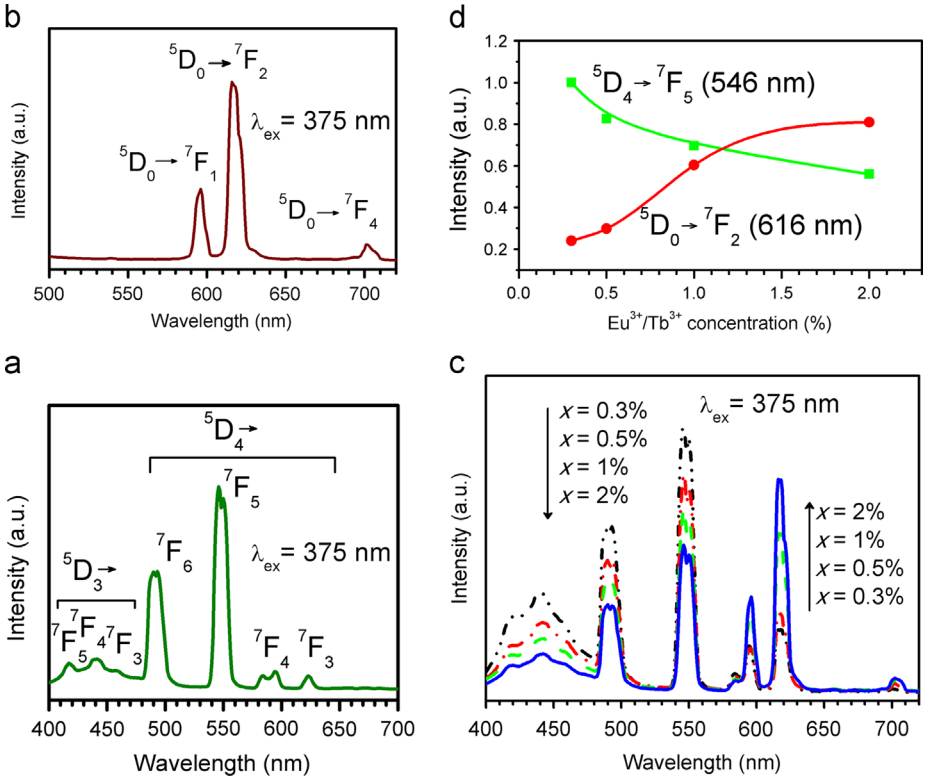

Fig. 7. PL spectra (λ_{ex}=375 nm) of (a) 0.5% Tb^{3+}-, (b) 2% Eu^{3+}- and (c) $x$$Eu^{3+}$/0.5% Tb^{3+} co-activated YAB phosphors. Figure (d) illustrate the variation of intensity of $^5D_4 \rightarrow {}^7F_5$ (Tb^{3+}) and $^5D_0 \rightarrow {}^7F_2$ (Eu^{3+}) transitions as a function of Eu^{3+}/Tb^{3+} concentration.

Tb^{3+} emission bands decreases and Eu^{3+} bands increases. The variation of intensity of Tb^{3+}:$^5D_4 \rightarrow {}^7F_5$ (546 nm) and Eu^{3+}:$^5D_0 \rightarrow {}^7F_2$ (616 nm) transitions as a function of Eu^{3+}/Tb^{3+} concentration is illustrated in Fig. 7d (as a reference). In case of Eu^{3+}/Tb^{3+} co-doped phosphors, the incorporation of 0.5% Tb^{3+} enhances the luminescence of Eu^{3+} by nearly 11% under 375 nm excitation than when excited with 395 nm wavelength. The decrease in intensity of Tb^{3+} emission bands and the enhancement of luminescence intensity of Eu^{3+} ion explore that the Tb^{3+} acts as an effective sensitizer by transferring the absorbed excitation energy to the Eu^{3+} ions in YAB phosphors.

Upon 375 nm excitation, few excited Tb^{3+} ions simultaneously decay radiatively through Tb^{3+}:$^5D_3 \rightarrow {}^7F_{5,4,3}$ transitions and non-radiatively (NR) to its lower lying Tb^{3+}:$^5D_4$ metastable state. The rest of the Tb^{3+} ions transfer their energy to the Eu^{3+}:$^5G_2$ level. A fast NR decay from $^5G_2$ excited state increase the population of $^5D_0$ metastable state causing enhanced emission from Eu^{3+} ions through $^5D_0 \rightarrow {}^7F_J$ transitions. Also, the overlapping of Eu^{3+}: $^7F_0 \rightarrow {}^5D_{3,2,1,0}$; Eu^{3+}:$^7F_1 \rightarrow {}^5D_{1,0}$; Eu^{3+}:$^7F_2 \rightarrow {}^5D_1$ excitation and Tb^{3+}:$^5D_3 \rightarrow {}^7F_{5,4,3}$; Tb^{3+}:$^5D_4 \rightarrow {}^7F_{5,4}$ emission transitions shown in Fig. 8 support the transfer of energy from Tb^{3+} to Eu^{3+} in YAB lattice. The transfer of energy from Tb^{3+} to Eu^{3+} takes place through different cross-relaxation (CR) channels shown below and are clearly illustrated in energy level diagram shown in Fig. 4.

A) $^5D_3$ (Tb^{3+})+$^7F_0$ (Eu^{3+})→$^7F_5$ (Tb^{3+})+$^5D_3$ (Eu^{3+})
B) $^5D_3$ (Tb^{3+})+$^7F_0$ (Eu^{3+})→$^7F_3$ (Tb^{3+})+$^5D_2$ (Eu^{3+})

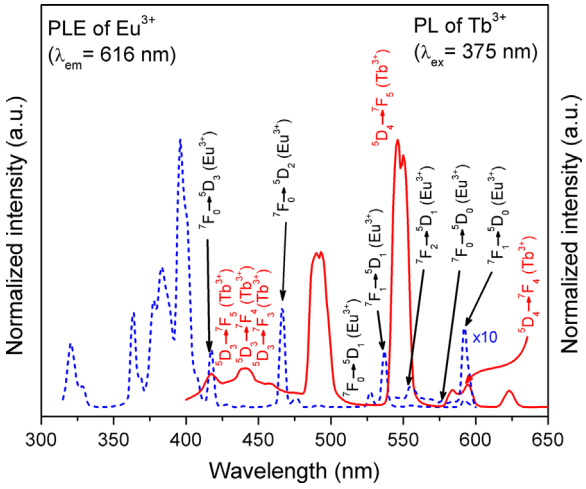

Fig. 8. Overlapping of Eu^{3+} excitation and Tb^{3+} emission transitions in YAB:$x$$Eu^{3+}$/0.5% Tb^{3+} phosphors.

C) $^5D_4$ (Tb^{3+})+$^7F_0$ (Eu^{3+})→$^7F_5$ (Tb^{3+})+$^5D_1$ (Eu^{3+})
D) $^5D_4$ (Tb^{3+})+$^7F_1$ (Eu^{3+})→$^7F_5$ (Tb^{3+})+$^5D_1$ (Eu^{3+})
E) $^5D_4$ (Tb^{3+})+$^7F_0$ (Eu^{3+})→$^7F_4$ (Tb^{3+})+$^5D_0$ (Eu^{3+})
F) $^5D_4$ (Tb^{3+})+$^7F_1$ (Eu^{3+})→$^7F_4$ (Tb^{3+})+$^5D_0$ (Eu^{3+})

The CIE chromaticity coordinates and corresponding emission color for YAB:$x$$Eu^{3+}$/0.5%$Tb^{3+}$ phosphors under 375 nm excitation are given in Table 1. These coordinates are well situated at their respective positions in CIE chromaticity diagram shown in Fig. 5. Upon 375 nm excitation, the

YAB:0.5%Tb^{3+} and YAB:2%Eu^{3+} phosphors exhibit pale-green and red luminescence, respectively. Conversely, the emission color of Eu^{3+}/Tb^{3+} co-doped phosphors could be changed from pale-green to white by increasing the Eu^{3+} concentration from 0.3% to 2%. The CIE chromaticity coordinates associated with white luminescence ($x=0.365$, $y=0.336$) of YAB:2% Eu^{3+}/0.5%Tb^{3+} phosphor are very close to an ideal white chromaticity coordinates ($x=0.333$, $y=0.333$). Moreover, the small value (i.e., less than unity) of $(({}^5D_0 \rightarrow {}^7F_1)/({}^5D_0 \rightarrow {}^7F_2))$ intensity ratio (see Table 1) under 375 nm excitation reveals that the Eu^{3+} and Tb^{3+} ions are embedded in low symmetry sites of YAB lattice. These results indicate that no structural changes take place around the luminescent centers (Eu^{3+} and/or Tb^{3+}) with excitation wavelength. However, the color tunability as a function of Eu^{3+}/Tb^{3+} concentration is mainly due to the combined luminescence effect of Eu^{3+} and Tb^{3+} ions.

To investigate the optical properties of YAB:$x$$Eu^{3+}$/0.5%$Tb^{3+}$ phosphors, the $\Omega_{2,4}$ intensity parameters and thus radiative properties have been evaluated using the Eqs. (4)–(8) and summarized in Table 3. In case of 375 nm excitation, the Ω_2 intensity parameter increases with the increase of Eu^{3+} concentration resulting more polarizable chemical environment suitable for emission color tunability from pale-green to white with narrow emission cross-section of $\sim 1.00\times10^{-21}$ cm^2. The magnitudes of radiative branching ratio (β_{Rad}) and luminescence decay time (τ_{Rad}) for YAB:2%Eu^{3+}/0.5%Tb^{3+} phosphors are almost the same to that obtained under 395 nm excitation. Upon 375 nm excitation, the Eu^{3+}:$^5D_0$ emission level exhibited the similar decay profiles when excited with 395 nm wavelength (not shown). The values of lifetime and luminescence quantum efficiency are listed in Table 3. Based on the above discussion, we suggest that the YAB:2%Eu^{3+} phosphor is potential for red solid-state lighting devices such as laser diodes, plasma display panels etc., and the YAB:2%Eu^{3+}/0.5%Tb^{3+} is potential for white LEDs. The emission color could be widely tuned from pale-green to white as a function of Eu^{3+}/Tb^{3+} concentration.

3.7. Energy transfer from Tb^{3+} to Eu^{3+} ions

The luminescence decay curve of $^5D_4$ emission level of Tb^{3+} ion in YAB:0.5%Tb^{3+} phosphor excited with 375 nm wavelength monitoring the emission at 546 nm ($^5D_4 \rightarrow {}^7F_5$) is presented in Fig. 9a. The lifetime is estimated to be ~3.19 ms by taking the first e-folding times of the intensity of decay curve. The decay profiles of $^5D_4$ (Tb^{3+}) emission state in the presence of Eu^{3+} ions are illustrated in Fig. 9b. All the decay profiles are well fitted to a second order exponential equation

$$I_{(t)} = A_1\exp(-t/\tau_1)+A_2\exp(-t/\tau_2) \quad (10)$$

where τ_1 and τ_2 represent the fast and slow lifetimes for the exponential components, respectively and A_1 and A_2 are corresponding constants. The average lifetime has been estimated using the formula, $\tau_{ave} = (A_1\tau_1^2+A_2\tau_2^2)/(A_1\tau_1+A_2\tau_2)$. The lifetime of $^5D_4$ (Tb^{3+}) level in Eu^{3+}/Tb^{3+} co-doped phosphors (see Table 4) decrease monotonically with the increase of Eu^{3+} concentration as depicted in Fig. 9c. This could be due to the ET from Tb^{3+} to Eu^{3+} ion. In case of co-doping of RE ions the quenching in luminescence has been due to the ET from donors to the acceptors until an energy sink is reached in the lattice [40]. Also, at critical concentration the average shortest distance between the nearest activator ions is equal to the critical transfer distance (R_c).

$$R_c \approx 2\left(\frac{3V}{4\pi x_c N}\right)^{1/3} \quad (11)$$

where V is the volume of the unit cell, x_c is the total critical concentration of dopant ions when the luminescence intensity of sensitizer decreases to its half that in the sample in the absence of activators and N is the number of available crystallographic sites per unit cell. For YAB phosphors, the values of N and V are 3 and 541.94 Å^3, respectively. For a total critical concentration of dopant ions ($x_c=2.5\%$), the critical transfer distance for efficient ET is found to be ~23.98 Å. The transfer of energy from Tb^{3+} to Eu^{3+} is higher for $x=2\%$ when compared to other concentrations. This can be confirmed by calculating the energy transfer efficiency (η_{ET}). In terms of lifetime, η_{ET} is given as [41]:

$$\eta_{ET}(\tau) = \left(1-\frac{\tau}{\tau_0}\right) \quad (12)$$

where τ and τ_0 are the corresponding lifetimes of sensitizer (Tb^{3+}) in the presence and absence of activator (Eu^{3+}) ion.

Table 3
J-O intensity parameters ($\Omega_{2,4}$) and radiative properties for $^5D_0 \rightarrow {}^7F_2$ (616 nm) transition of Eu^{3+} ion in YAB:$x$$Eu^{3+}$/0.5%$Tb^{3+}$ phosphor s under 375 nm excitation.

Parameter	YAB:2% Eu^{3+}	YAB:$x$$Eu^{3+}$/0.5%$Tb^{3+}$ ($\lambda_{ex}=375$ nm)			
		$x=0.3\%$	$x=0.5\%$	$x=1\%$	$x=2\%$
Ω_2 ($\pm 0.20\times10^{-20}$ cm^2)	4.78	2.92	3.14	3.85	4.30
Ω_4 ($\pm 0.04\times10^{-20}$ cm^2)	0.79	0.36	0.67	0.56	0.66
$\Delta\lambda_{eff}$ (nm)	9.09	11.21	10.20	9.75	9.43
A_{Rad}(s^{-1})	218.90	133.72	143.89	176.25	196.93
β_{Rad}	0.72	0.64	0.63	0.68	0.70
τ_{Rad}(ms)	3.29	4.77	4.41	3.89	3.58
σ_{emis}($\times10^{-21}$ cm^2)	1.59	0.79	0.93	1.19	1.38
τ_{meas}(ms)	1.38	2.05	1.85	1.73	1.50
η_{QE}(%)	42	43	42	44	42

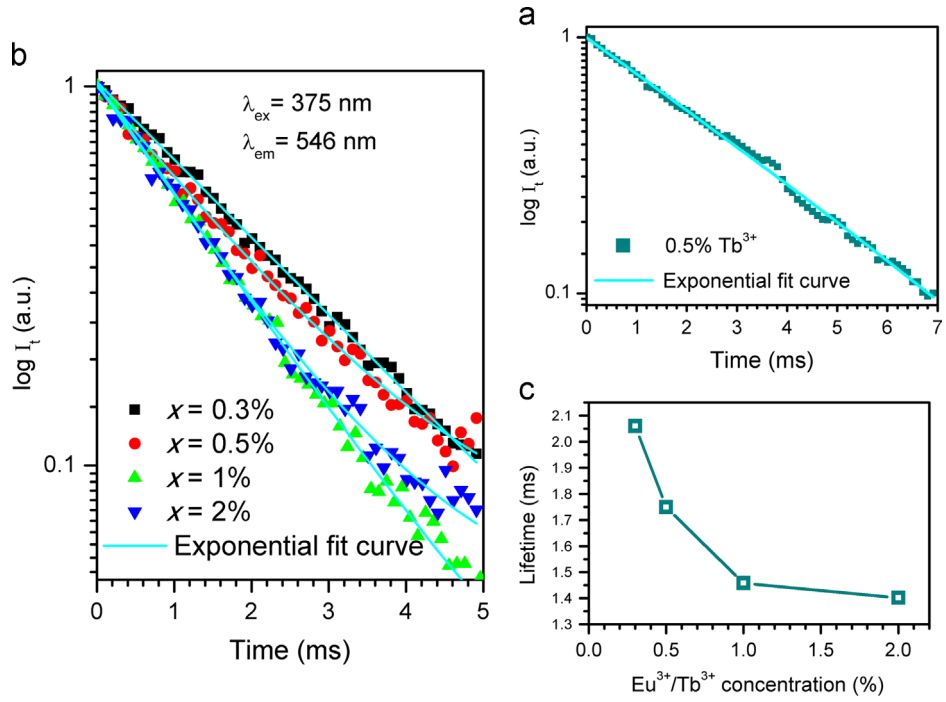

Fig. 9. Luminescence decay profiles of (a) 0.5% Tb^{3+}- and (b) xEu^{3+}/0.5% Tb^{3+} co-doped YAB phosphors. Figure (c) is the lifetime of $^5D_4$ (Tb^{3+}) state vs. Eu^{3+}/Tb^{3+} concentration.

Table 4
Measured lifetime (τ_{meas}) of $^5D_4$ emission state of Tb^{3+}, energy transfer efficiency (η_{ET}) and energy transfer rate (ρ_{ET}) from Tb^{3+} to Eu^{3+} in YAB: xEu^{3+}/0.5%Tb^{3+} phosphors under 375 nm excitation.

YAB doping	τ_{meas} (ms)	ρ_{ET}	ET efficiency (in %)	
			$\eta_{ET}(\tau)$	$\eta_{ET}(I)$
$x=0$	3.19	–	–	–
$x=0.3\%$	2.12	161	34	37
$x=0.5\%$	1.69	278	47	52
$x=1\%$	1.48	368	54	59
$x=2\%$	1.41	399	56	67

The energy transfer rate (ρ_{ET}) from sensitizer to activator ion has been calculated using the formula [42]:

$$\rho_{ET} = \frac{\eta_{ET}}{(1-\eta_{ET})\,\tau_0} \tag{13}$$

According to Förster [43], the energy transfer efficiency in terms of luminescence intensity is given by

$$\eta_{ET}(I) = \left(1 - \frac{I}{I_0}\right) \tag{14}$$

where I and I_0 are the corresponding luminescence intensities of sensitizer (Tb^{3+}) in the presence and absence of activator (Eu^{3+}) ion. The values of energy transfer efficiency evaluated from the lifetime ($\eta_{ET}(\tau)$) and luminescence intensities ($\eta_{ET}(I)$) and energy transfer rates (ρ_{ET}) from Tb^{3+} to Eu^{3+} ion are given in Table 4. The magnitudes of ET efficiency calculated from the lifetime measurements are very close to that obtained from the luminescence intensities. As seen the η_{ET} and ρ_{ET} values, the Tb^{3+} ions act as an efficient sensitizer of luminescence of Eu^{3+} in YAB lattice. In order to know the type of interactions (s) through which the ET from Tb^{3+} to Eu^{3+} ions take place, the intensity of Tb^{3+}:$^5D_4 \rightarrow {}^7F_5$ (546 nm) transition has been integrated from the emission spectra of YAB:xEu^{3+}/0.5%Tb^{3+} phosphors shown in Fig. 7c. The relationship between the luminescence intensity of the donor ions (Tb^{3+}) and the concentration (C) of the acceptor ions (Eu^{3+}) satisfies the following equation [44]:

$$\frac{I}{I_0} = (1 + AC^{s/3})^{-1}$$

$$(or)\ \log\left(\frac{I}{I_o}\right) = \frac{s}{3}\log C + \log A \tag{15}$$

where I and I_0 are the luminescence intensity of donor ions (Tb^{3+}) in the presence and absence of acceptor ions (Eu^{3+}), respectively and A is a constant for the selected host and is independent of the doping concentration. The electric multi-pole interaction parameter (s) taking the values 3 (exchange), 6 (dipole-dipole), 8 (dipole-quadrupole), and 10 (quadrupole-quadrupole) can be calculated from the slop of log [$I/I_{0(Tb)}$] vs. log (C_{Eu}) curve. For Tb^{3+}:$^5D_4 \rightarrow {}^7F_5$ transition, the log [$I/I_{0(Tb)}$] vs. log (C_{Eu}) plot is shown in Fig. 10. The slop parameter (s/3) can be calculated by fitting the experimental data to a linear equation: $y = -(1.03 \pm 0.06)\,x - (2.47 \pm 0.12)$. From this equation, the value of 's' is found to be ~3 which reveals that the transfer of energy from Tb^{3+} to Eu^{3+} takes place through exchange interaction mechanism. However, the exchange interaction mechanism is ineffective when the ion-ion distances are larger than 4 or 5 Å [40]. Malta [45] stated that the exchange interaction mechanism strongly depends on the overlap integral between donor and acceptor 4f sub-shells and it is possible for ion-ion distances larger than 4 Å in the presence of clustering effect only. To know the clustering effect the average distance

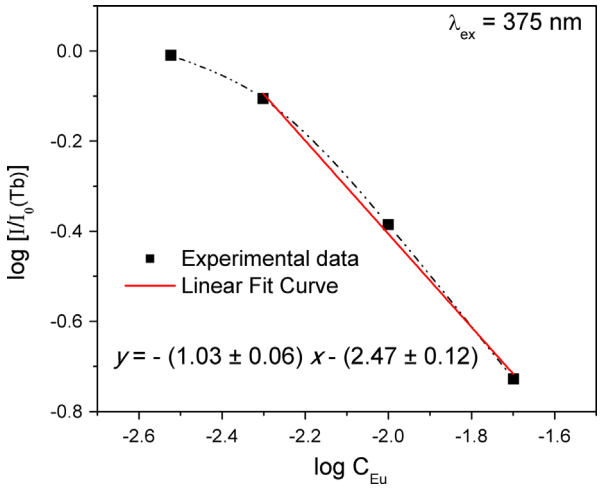

Fig. 10. Log($I/I_{0(Tb)}$) versus log C_{Eu} plot for YAB:xEu^{3+}/0.5%Tb^{3+} phosphors.

(R_{ran}) between Tb^{3+} and Eu^{3+} ions assuming a random distribution of ions has been determined using the following formula [46]:

$$R_{ran} = 2\left(\frac{3}{4\pi(C_{Tb}+C_{Eu})}\right)^{1/3} \quad (16)$$

where C_{Tb} and C_{Eu} are the total concentrations of Tb^{3+} (2.54×10^{19} ions/cm^3) and Eu^{3+} (1.02×10^{20} ions/cm^3) ions, respectively. The value of R_{ran} is ~24.63 Å which is found slightly higher than the critical transfer distance (R_c = 23.98 Å) between Tb^{3+} and Eu^{3+} ions. The higher value of R_{ran} confirms the formation of Eu^{3+}-Tb^{3+} clusters in YAB lattice. Hence, the transfer of energy from Tb^{3+} to Eu^{3+} takes place in Eu^{3+}-Tb^{3+} clusters instead of from these ions randomly distributed. Further to know the effect of size of nanoparticles on the luminescence, the YAB:Eu^{3+}/Tb^{3+} phosphors have to be synthesized following sol-gel, hydrothermal and other advanced techniques.

4. Conclusions

The effect of sensitization of Tb^{3+} ion on the luminescence of Eu^{3+} was systematically investigated in Eu^{3+}/Tb^{3+} co-doped YAB phosphors prepared by solid-state reaction method. The Eu^{3+}/ Tb^{3+} co-doped phosphors have shown their luminescence properties in their respective emission regions and exhibit tunable emission from green to white to red with excellent CIE chromaticity coordinates. The YAB:2% Eu^{3+} phosphor emits red luminescence ($^5D_0\rightarrow{}^7F_2$) with CIE chromaticity coordinates (x=0.627, y=0.334) which are very close to an ideal red (x=0.67, y=0.33) and commercial Y_2O_3:Eu^{3+} red phosphor (x=0.64, y=0.34) chromaticity coordinates. The chromaticity coordinates associated with white luminescence (x=0.365, y=0.336) of YAB:2%Eu^{3+}/0.5% Tb^{3+} phosphor (λ_{ex}=375 nm) are also close to an ideal white chromaticity coordinates (x=0.333, y=0.333). In case of Eu^{3+}/Tb^{3+} co-activated phosphors, the energy transfer from Tb^{3+} to Eu^{3+} ions takes place through exchange interaction mechanism in Eu^{3+}-Tb^{3+} clusters instead of from these ions randomly distributed in YAB phosphor due to the effective sensitization of Tb^{3+}. Based on the observed results and a wide range of color tunability from pale-green to white as confirmed by the CIE chromaticity diagram, we suggest that the YAB:Eu^{3+}/Tb^{3+} phosphors have potential for display devices.

Acknowledgments

One of the authors Dr. B.C. Jamalaiah would like to thank the Fundação para a Ciência e a Tecnologia (FCT), Ministério da Educação e Ciência, PORTUGAL for supporting him as a Post-Doctoral Researcher wide Ref. no. SFRH/BPD/76581/2011.

References

[1] P. Schlotter, R. Schmidt, J. Schneider, Luminescence conversion of blue light emitting diodes, Applied Physics A 64 (1997) 417–418.
[2] S. Nakamura, S. Pearton, G. Fasol, The Blue Laser Diode, first ed., Springer-Verlag, New York, 1997.
[3] Y.-C. Liao, C.-H. Lin, S.-L. Wang, Direct white light phosphor: a porous zinc gallophosphate with tunable yellow-to-white luminescence, Journal of the American Chemical Society 127 (2005) 9986–9987.
[4] T. Wang, Y.H. Liu, Y.B. Lee, J.P. Ao, J. Bai, S. Sakai, 1 mW AlInGaN-based ultraviolet light-emitting diode with an emission wavelength of 348 nm grown on sapphire substrate, Applied Physics Letters 81 (2002) 2508.
[5] J. Jeong, M. Jayasimhadri, H.-S. Lee, K. Jang, S.-S. Yi, J.-H. Jeong, C. Kim, Photoluminescence and phosphorescence properties of $Sr_{1-x}Zn_{2-y}(PO_4)_2$:Eu_x^{2+};Mn_y^{2+} phosphor for UV-based white-LEDs, Physica B 404 (2009) 2016–2019.
[6] J.-H. Park, N.-G. Back, M.-G. Kwak, B.-E. Jun, B.-C. Choi, B.-K. Moon, J.-H. Jeong, S.-S. Yi, J.-B. Kim, Synthesis and properties of luminescent Y_2O_3: Tb^{3+}(5, 8, 12 wt%) nanocrystals, Materials Science and Engineering C 27 (2007) 9981001.
[7] J.M. Sung, S.E. Lin, W.C.J. Wei, Synthesis and reaction kinetics for monodispersive Y_2O_3:Tb^{3+} spherical phosphor particles, Journal of the European Ceramic Society 27 (2007) 2605–2611.
[8] X. Zhenxiu, H. Zhanglian, Z. Qichao, P. Lixia, Z. Pengyue, Preparation and luminescence properties of Y_2O_3:Eu^{3+} nanorods via post annealing process, Journal of Rare Earths, 24, , 2006, p. 111–114.
[9] A.H. Kitai, Oxide phosphor and dielectric thin films for electroluminescent devices, Thin Solid Films 445 (2003) 367–376.
[10] Z.-W. Zhang, X.-Y. Sun, D.-D. Jia, S.-T. Song, J.-P. Zhang, S.-F. Wang, Tunable full color emission from single-phase $LiSr_{3.99-x}Dy_{0.01}(BO_3)_3$: $_xEu^{3+}$ phosphors, Ceramics International 39 (2013) 3965–3970.
[11] B. Han, J. Zhang, Q. Cui, Y. Liu, A Potential Reddish Orange Emitting Phosphor Ca_2BO_3Cl:Eu^{3+} for White Light-Emitting Diodes, Physica B 407 (2012) 3484–3486.
[12] G.V.L. Reddy, L.R. Moorthy, B.C. Jamalaiah, T. Sasikala, Preparation, structural and luminescent properties of $YAl_3(BO_3)_4$:Dy^{3+} phosphor for white light-emission under UV excitation, Ceramics International 39 (2013) 2675–2682.
[13] J.L. Yuan, J. Wang, D.B. Xiong, J.T. Zhao, Y.B. Fu, G.B. Zhang, C.S. Shi, Potential PDP phosphors with strong absorption around 172 nm: rare earth doped $NaLaP_2O_7$ and $NaGdP_2O_7$, Journal of Luminescence 126 (2007) 717–722.
[14] H. Yamamoto, K. Urabe, Host sensitization mechanism of Eu^{3+} luminescence in $(Y,In)_2O_3$, Journal of Electrochemical Society 129 (1982) 2069–2074.
[15] E. Pavitra, G.S.R. Raju, Y.H. Ko, J.S. Yu, A Novel, Strategy for controllable emissions from Eu^{3+} or Sm^{3+} ions co-doped SrY_2O_4:Tb^{3+} phosphors, Physical Chemistry Chemical Physics 14 (2012) 11296–11307.

[16] S. Som, S.K. Sharma, Eu^{3+}/Tb^{3+} co-doped Y_2O_3 nanophosphors: rietveld refinement, band gap and photoluminescence optimization, Journal of Physics D: Applied Physics 45 (2012) 415102.
[17] G.A. Sotiriou, M. Schneider, S.E. Pratsinis, Color-Tunable Nanophosphors by Codoping Flame-Made Y_2O_3 with Tb and Eu, The Journal of Physical Chemistry C 115 (2011) 1084–1089.
[18] D. Tu, Y. Liang, R. Liu, D. Li, Eu/Tb ions co-doped white light luminescence Y_2O_3 phosphors, Journal of Luminescence 131 (2011) 2569–2573.
[19] D. Wang, Y. Wang, J.-W. He, Investigation of energy absorption and transfer process of Tb^{3+} or Eu^{3+} excited $Na_3Gd(PO_4)_2$ in the VUV region, Materials Research Bulletin 47 (2012) 142–145.
[20] L. Chen, Y. Fu, G. Zhang, J. Bao, C. Gao, Optimization of Pr^{3+}, Tb^{3+} and Sm^{3+} co-doped $(Y_{0.65}Gd_{0.35})BO_3:Eu^{3+}_{0.05}$ VUV phosphors through combinatorial approach, Journal of Combinatorial Chemistry 10 (2008) 401–404.
[21] F. Xiao, Y.N. Xue, Q.Y. Zhang, $Y_4MgSi_3O_{13}:RE^{3+}$ (RE=Ce, Tb and Eu) nanophosphors for a full-color display, Physica B 405 (2010) 4445–4449.
[22] E.L. Belokoneva, A.V. Azizov, N.I. Leonyuk, M.A. Simonov, N.V. Belov, Crystal Structure of $YAl_3[BO_3]_4$, Zhurnal Strukturnot Khtmit 22 (1981) 476–478.
[23] L.J.Q. Maia, A. Ibanez, L. Ortega, V.R. Mastelaro, A.C. Hernandes, Er:YAB nanoparticles and vitreous thin films by the polymeric precursor method, Journal of Nanoparticles Research 10 (2008) 1251–1262.
[24] J. Madarasz, E. Beregi, J. Sztatisz, I Földvari, G Pokol, Combined DTA and XRD study of sintering steps towards $YAl_3(BO_3)_4$, Journal of Thermal Analysis and Calorimetry 64 (2001) 1059–1065.
[25] P. Singh, A. Kumar, A. Kaushal, D. Kaur, A. Pandey, R.N. Goyal, In situ high temperature XRD studies of ZnO nanopowder prepared via cost effective ultrasonic mist chemical vapour deposition, Bulletin of Materials Science 31 (2008) 573–577.
[26] L.-L. Zhang, C.-X. Guo, J.-J. Zhao, J.-T. Hu, Photoluminescence of Eu (III) -doped ZnO nanopowder and energy transfer from ZnO to Eu(III) ions, Chinese Physics Letters 22 (2005) 1225–1227.
[27] W.T. Carnall, P.R. Fields, K. Rajnak, Electronic energy levels of the trivalent lanthanide aquo ions IV Eu^{3+}, Journal of Chemical Physics 49 (1968) 4450–4455.
[28] W.T. Carnall, P.R. Fields, K. Rajnak, Electronic energy levels of the trivalent lanthanide aquo ions III Tb^{3+}, Journal of Chemical Physics 49 (1968) 4447–4449.
[29] S. Mukherjee, V. Sudarsan, R.K. Vatsa, S.V. Godbole, R.M. Kadam, U.M. Bhatta, A.K. Tyagi, Effect of structure, particle size and relative concentration of Eu^{3+} and Tb^{3+} ions on the luminescence properties of Eu^{3+} co-doped Y_2O_3:Tb nanoparticles, Nanotechnology 19 (2008) 325704.
[30] G. Blasse, On the Eu^{3+} fluorescence of mixed metal oxides. IV. the photoluminescent efficiency of Eu^{3+} activated oxides, Journal of Chemical Physics 45 (7) (1966) 2356–2360.
[31] O.L. Malta, H.F. Brito, J.F.S. Menezes, F.R. Gongalves e Silva, S. Alves Jr., F.S. Farias Jr., A.V.M. de Andrade, Spectroscopic properties of a new light-converting device Eu(thenoyltrifluoroacetonate)$_3$ 2(dibenzyl sulfoxide). A theoretical analysis based on structural data obtained from a sparkle model, Journal of Luminescence 75 (1997) 255–268.
[32] O.L. Malta, M.A. Couto dos Santos, L.C. Thompson, N.K. Ito, Intensity parameters of 4f–4f transitions in the Eu (dipivaloylmethanate)$_3$ 1, 10-phenanthroline complex, Journal of Luminescence 69 (1996) 77–84.
[33] L.J.Q. Maia, Valmor R. Mastelaro, Sebastien Pairis, Antonio C. Hernandes, A Alain Ibanez, Sol–gel route for the development of rare-earth aluminum borate nanopowders and transparent thin films, Journal Solid State Chemistry 180 (2007) 611–618.
[34] H. Ebendorff-Heidepriem, D. Ehrt, Spectroscopic properties of Eu^{3+} and Tb^{3+} Ions for local structure investigations of fluoride phosphate and phosphate glasses, Journal of Non-Crystalline Solids 208 (1996) 205–216.
[35] M. Kumar, T.K. Seshagiri, M. Mohapatra, V. Natarajan, S.V. Godbole, Synthesis, characterization and studies of radiative properties on Eu^{3+} -doped $ZnAl_2O_4$, Journal of Luminescence 132 (2012) 2810–2816.
[36] F. Lei, B. Yan, Hydrothermal synthesis and luminescence of $CaMO_4:RE^{3+}$ (M=W, Mo; RE=Eu, Tb) sub micro-phosphors, Journal of Solid State Chemistry 181 (2008) 855–862.
[37] B.R. Judd, Optical Absorption Intensities of Rare-earth Ions, Physical Review 127 (1962) 750–755.
[38] G.S. Ofelt, Intensities of crystal spectra of rare-earth ions, Journal of Chemical Physics 37 (1962) 511–514.
[39] Y. Tian, X. Qi, X. Wu, R. Hua, B. Chen, Luminescent properties of $Y_2(MoO_4)_3:Eu^{3+}$ red phosphors with flowerlike shape prepared via co-precipitation method, Journal of Physical Chemistry C, 113, 2009, p. 10767–10772.
[40] G. Blasse, Energy transfer in oxide phosphors, Physics Letters A 28 (1968) 444–445.
[41] P.I. Paulose, G. Jose, V. Thomas, N.V. Unnikrishnan, M.K.R. Warrier, Sensitized fluorescence of Ce^{3+}/Mn^{2+} system in phosphate glass, Journal of Physics and Chemistry of Solids 64 (2003) 841–846.
[42] U. Caldiño, J.L. Hernández-Pozos, C. Flores, A. Speghini, M. Bettinelli, Photoluminescence of Ce^{3+} and Mn^{2+} in zinc metaphosphate glasses, Journal of Physics: Condensed Matter 17 (2005) 7297–7305.
[43] Th. Förster, Transfer mechanisms of electronic excitation energy, Radiation Research Supplement 2 (1960) 326–339.
[44] L.G. Van Uitert, Characterization of energy transfer interactions between rare earth ions, Journal of Electrochemical Society 114 (1967) 1048–1053.
[45] O.L. Malta, Mechanisms of non-radiative energy transfer involving lanthanide ions revisited, Journal of Non-Crystalline Solids 354 (2008) 4770–4776.
[46] R. Martínez-Martínez, M. García, A. Speghini, M. Bettinelli, C. Falcony, U. Caldiño, Blue–green–red luminescence from $CeCl_3$- and $MnCl_2$-doped hafnium oxide layers prepared by ultrasonic spray pyrolysis, Journal of Physics: Condensed Matter 20 (2008) 395205.